Janaraj, Thangarajah & Dhanasekar, Manicka
(2014)
Finite element analysis of the in-plane shear behaviour of masonry panels confined with reinforced grouted cores.
Construction and Building Materials, *65*, pp. 495-506.

Finite element analysis of the in-plane shear behaviour of masonry panels confined with reinforced grouted cores

Thangarajah Janaraj[1], Manicka Dhanasekar[2]

School of Civil Engineering and Built Environment, Queensland University of Technology, Australia.

Abstract

A combined experimental and numerical program was conducted to study the in-plane shear behaviour of hollow concrete masonry panels containing reinforced grout cores. This paper is focused on the numerical program. A two dimensional macro modelling strategy was used to simulate the behaviour of the confined masonry (CM) shear panels. Both the unreinforced masonry and the confining element were modelled using macro masonry properties and the steel reinforcement was modelled as an embedded truss element located within the grout using perfectly bonded constraint. The FE model reproduced key behaviours observed in the experiments, including the shear strength, the deformation and the crack patterns of the unconfined and confined masonry panels. The predictions of the validated model were used to evaluate the existing in-plane shear expressions available in the national masonry standards and research publications.

Keywords: Finite element, Diagonal testing, In-plane shear, Confined masonry, In-plane shear equations.

1. Introduction

Earthquake and severe tropical cyclones (typhoons) are the major natural disasters, facing the mankind; designing buildings to withstand to these natural disasters requires careful attention to the potential for higher demand of in-plane shear load and brittle shear failure. Where the demand exceeds the capacity of the shear walls, the entire building may be destroyed allowing less time to dwellers to evacuate. The in-plane shear analysis usually considers the slabs as rigid diaphragms to distribute the lateral forces to shear walls.

[1] janaraj.thangarajah@student.qut.edu.au
[2] m.dhanasekar@qut.edu.au (Corresponding Author)

Masonry is perhaps the least understood oldest major construction material as far as its structural in-plane behaviour is concerned. Unreinforced Masonry (URM) buildings are designed mainly for gravity loads and their capacity to in-plane load is generally inadequate. To overcome this inadequacy, a grid of horizontal and vertical reinforced grout elements that break a large masonry wall into smaller panels can be introduced; these elements can effectively confine URM panels. This type of masonry wall construction, known as confined masonry, is shown to outperform other types of masonry constructions in seismic zones [1, 2]. In this type of construction the unreinforced masonry panels with specific recesses for placing reinforcement is constructed first followed by pouring concrete into these recesses. This type of construction has similarity to partially grouted (or wide spaced reinforced) masonry shear walls adopted in Australia and most parts of North America [3, 4]. The load resisting capacity of the confined masonry is maintained until the masonry panels experience severe cracking. Significant lateral deformation and ductility can thus be attained before the collapse.

The in-plane shear capacity of the walls can be determined using cost-effective numerical tools because such tools can be useful to model walls with differing parameters that can be evaluated through standard testing on masonry sub-assemblages (as against full scale structural walls).

The diagonal compression test is an elegant and adequate approach to evaluate the masonry properties [1, 5, 6]. It is also widely being used to evaluate the effectiveness of damaged/ undamaged panels strengthened using different techniques [7-9]. The diagonal compression test results have also been used to validate the Finite Element (FE) models [8, 10]. Generally the diagonal compression test panel failures are more brittle than those observed in shear wall tests; therefore, they can be considered as lower bound (conservative) testing method.

Numerical studies on masonry shear walls have been carried out in two different levels; a) micro level, and b) macro level. The micro modelling is devoted to develop reliable interface deformation and failure mechanisms through the theories of plasticity or fracture mechanics. Using multi surface plasticity models Lourenço and Rots [11], Gambarota and Lagomarsino[12], and van Zijl[13] successfully predicted the inplane shear capacity of horizontally loaded walls.

Using the model developed by Lourenço and Rots [11], Petersen et al.[8] attempted to validate diagonally loaded URM panels (with and without FRP strengthening) in DIANA

platform and succeeded in predicting the peak load but failed to predict post peak behaviour; they could not predict the brittle failure exhibited by the diagonally loaded URM panels in the experiment using their FE model, which reported ductile response unconservatively. Similar 2-D micro modelling attempt was made by Gabor et al.[10] for diagonally loaded URM panels that resulted in similar outcomes as that of Peterson et al. [8].

Sousa et al.[14] developed a 3-D approach using similar micro modelling concept for diagonal loaded URM panels; again their FE model exhibited higher ductile response than that of their experiment test results. Despite the prediction of peak load capacity of diagonally loaded wall panels, this micro modelling technique is quite laborious and require careful definition of contact interfaces; when considering hollow block grouted masonry, there are far too many interfaces and this approach becomes impractical if not impossible.

The macro modelling technique can be applied to large size masonry walls with ease. The downside is that it requires homogenised material properties. To date, no attempts were made to simulate the response of the diagonally loaded hollow concrete masonry panels using macro modelling technique. This paper contains the details of an adapted macro modelling approach for unconfined and confined masonry panels tested under diagonal compression, which successfully predicted the failure mode, shear strength and deformation characteristics.

Empirical formulae are provided in many national masonry standards [15-18] and research papers [19, 20] for reinforced masonry shear capacity prediction. Most of these design expressions are formulated from small scale tests conducted in the laboratories and/ or based on the experience of designers. The Australian Masonry standard (AS3700) [16] has attracted many criticisms from researchers as its predictions remain highly un-conservative [4, 21-23]. Relatively, the predictions made by MSJC-2008[15], CSA:S304.1-2004[17] and NZS4230-2004[18] are less criticised, in few occasions their predictions are reported as reasonable for small experimental walls [24]. These criticisms may be attributed to the inherent variability in masonry and the large number of parameters that affect the behaviour of shear walls.

This paper describes calibration of a macro modelling method from the response of diagonally loaded unconfined and confined masonry panels determined from experiments and then using the FE model to predict the behaviour of horizontally loaded reinforced masonry shear panels. The predictions of the validated model were used to evaluate the existing in-plane shear expressions available in the national masonry standards and research publications.

2. Experimental program

A testing program was undertaken to calibrate the FE model. These testing programs contained 55 small scale test specimens to characterise the material properties of the masonry assemblages. Four diagonally loaded unconfined and confined masonry panels were tested to validate the FE model predictions. All these test specimens were constructed using half scale hollow blocks of dimensions 185mm×90mm×90.5mm (length×height×width) manufactured in Canada and imported to Australia.

2.1. Characterisation of Materials

All material tests were carried out on half scale specimens. All specimens were tested in 14 days except the grout cylinders (which were tested on the 28th day). First 7days were cured under control environment then next seven days were allowed air curing. The mortar thickness was reduced to 5mm and hence the fine aggregates used in the mortar were scaled down accordingly. In the grout, 10 mm aggregates were used with scaled down fine aggregates. Very high slump value of 260mm was used in order to self-compact the poured grout into hollow masonry recesses. The compressive strength of the grout (f_c) was determined from 12 specimens tested in accordance with AS3600.

The block unconfined compressive strength (f_{uc}) was determined by testing six specimens in accordance with the AS/NZS:4456.4. The average elastic modulus of the block (E_b) was determined from the gradient of the stress-strain curves. The modulus of the rupture of the block (f_{ut}) was determined from 8 specimens (3 blocks attached along the head joints) in accordance with AS/NZS-4456.15. The compressive strength of the hollow masonry ($f_{hmc\perp}$) and the grouted masonry ($f_{gmc\perp}$) was conducted from 12 and 6 prisms (4 bricks high masonry sub assemblages), respectively in accordance withAS3700[16]. Five mm thick *M3*(1:1:6-cement:lime: sand) mortar was used. The elastic modulus of the hollow masonry ($E_{hmc\perp}$) and grouted masonry ($E_{gmc\perp}$) were determined from the stress-strain curves obtained from the compression tests. The flexural tensile strength of hollow masonry (f_{mt}) was conducted from seven blocks long masonry beams in accordance with AS3700[16]. The masonry shear bond strength (f_{ms}) was determined by testing three masonry triplets in accordance with EN.1052-

3. The tensile coupon tests were carried out on N12 reinforcement bar to determine its yield strength (f_{ys}) and Elastic modulus (E_s). No tests were conducted on mortar. However the ratio of cement, lime and sand was kept constant throughout the entire test (*M3* mortar). The mortar modulus of elasticity (E_m) was determined using Eq.1.

$$E_m = \frac{E_{hmc\perp}}{\beta(E_b - E_{hmc\perp}) + E_b} \quad (1)$$

In which β is ratio of block height to mortar thickness. The mean results of the masonry constituent materials and assemblages along with the obtained minimum and maximum values are reported in Table 1.

Table 1.Material properties

Test details	No.of specimens	Mean (*MPa*)	Minimum (*MPa*)	Maximum (*MPa*)	COV (%)
f_c	12	30.1	29.1	32.5	6
f_{uc}	6	18.7	16.5	20.8	7.4
E_b	6	3304	2625	3618	10.9
f_{ut}	8	2.8	2.3	2.9	10.9
$f_{hmc\perp}$	12	9.2	6.9	11	16
$E_{hmc\perp}$	12	3277	2155	4400	28
$f_{gmc\perp}$	6	8.8	6.6	10.4	17.2
$E_{gmc\perp}$	6	14592	11900	18783	22
f_{mt}	6	0.5	0.32	0.62	22
f_{ms}	3	0.6	0.58	0.61	2.6
E_m	-	2840	-	-	-
f_{ys}	2	500	-	-	-
E_s	2	200, 000	-	-	-

Typical failure patterns of the masonry sub assemblages are shown in Fig. 1.

a) Modulus of rupture test on blocks

b) Compressive test (hollow)

c) Compressive test (grout)

d) Flexural tensile test on masonry

e) Triplet test

Figure 1.Typical failure of masonry sub assemblages.

2.2. Panel specimens

This experimental program consists of two unconfined masonry panels and two confined masonry panels. Both the unconfined masonry panels are denoted as UCM-A and UCM-B; and the confined masonry panels are denoted as CM-A and CM-B. The dimension of the 850mm×850mm half scale square panels was considered such that it contained adequate number of mortar units and joints. This half scale panels represent an actual wall size of 1700mm×1700mm. The confined masonry panel contains grout in its edge recesses with 1N12 (12mm diameter, normal ductility bar of 500MPa yield strength) bar embedded in each grouted core. Typical dimension and the geometric details of the panels are shown in Fig. 2.

ASTM-E519-02[25] does not suggest diagonal compression test for confined masonry. However, it should be noted that this testing was used more as a proof of concept of the appropriateness of conducting diagonal compression tests for confined masonry panels rather than estimating their shear parameters. The reinforcement (iN12) was placed at the center of each grouted core to eliminate eccentricity. The pouring of grout in the edge recesses was carried out during the construction of the masonry panels.

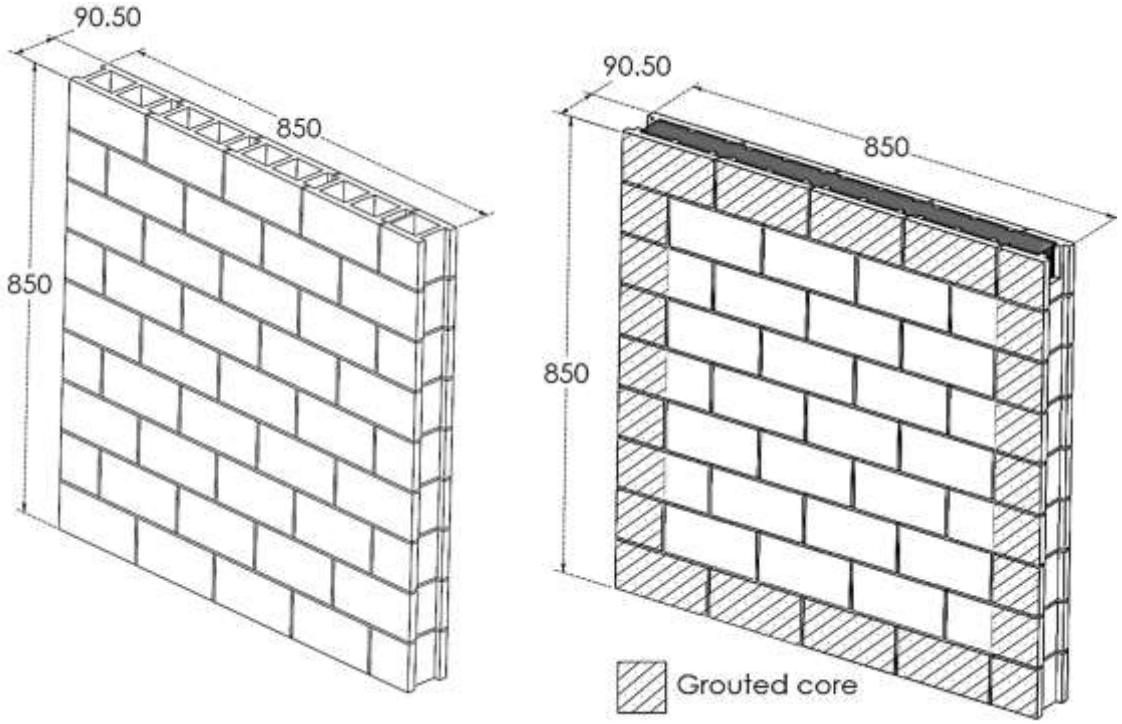

a) UCM panel b) CM panel

Figure 2. Masonry panels geometry

2.3. Test set-up

ASTM-E519-02[25] standard guidelines were used to design the test set-up. This test procedure provided simple means of producing diagonal cracking and sliding failure modes in order to validate the FE model. Displacement controlled loading was applied to study the softening behaviour. The displacement was applied at a rate of 1mm/min. From the actuator sensors, applied diagonal force and the displacement were recorded. The test set-up is shown in Fig. 3. 235 kN each dual synchronised hydraulic actuators were used. Potentiometers were attached on both sides of the panels as shown in Fig. 4. The average responses were

considered to eliminate any potential eccentricity through the thickness direction of the panel. LVDT1 and LVDT2 measured the vertical displacement applied on top of the loading shoe. LVDT3 monitored any out-of-plane movement of the panel during the loading.

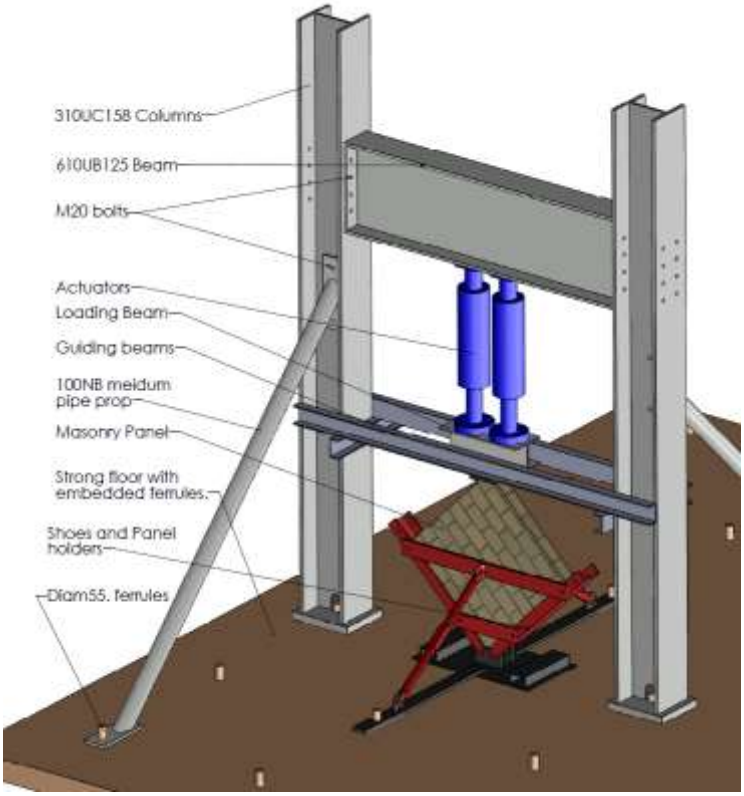

Figure 3. Test set-up.

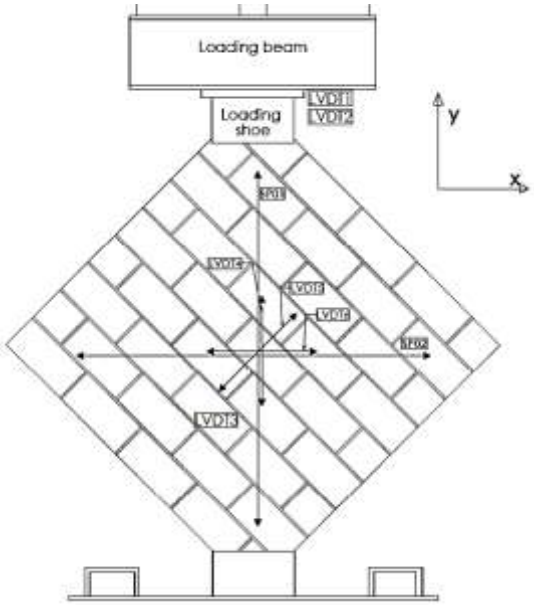

Figure 4. Schematic diagram of instrumentation

LVDTs 4-6 measured the response at middle of the panels. SP01 and SP02 are resistance controlled string pots; they measured the diagonal displacement of the panels. These readings were used to estimate the shear modulus.

3. Numerical implementation

FE modelling approach is discussed in this section. This FE analyses were performed using ABAQUS/Explicit[26] macro modelling VUMAT adapted from Haider[21]. The panels were modelled in two dimensions using plane stress elements to study their in-plane shear behaviour.

3.1 Masonry model

The hollow masonry was modelled using smeared properties of all of its components. Using this approach, the pre-peak and post-peak responses of the masonry panel were studied until the ultimate failure of the panel occurred. This model can be used to model large walls with ease as long as the appropriate material properties of the smeared masonry is known as a priori to uncover the effect of confinement of the grouted reinforced element to the unreinforced masonry panels in large walls; such information will be of significant practical value and can potentially eliminate the un-conservativeness of the analytical expressions provided in the national masonry design standards.

The anisotropy of masonry composite arose from the geometrical arrangement of units and mortar in a typical wall. Several researchers have carried out experimental investigations to identify the failure surface for masonry panels under uni-axial and bi-axial conditions [27, 28]. Seim[29] and Lourenço et al. [30] adopted modern plasticity theories to analytically formulate the yield surfaces for masonry.

The multisurface plasticity model proposed by Lourenço[31] was adopted for masonry modelling. For the compression, hill type failure surface was adopted, as shown in Fig. 5. For the tension Rankine type failure surface was adopted as shown in Fig. 6.

One of the major disadvantages of macro modelling is that incorporates smeared crack modelling which causes localisation leading to mesh size dependence (or, mesh pathology). A multi-dimensional non-local theory to cater for the orthotropy of the masonry would be more complex and hence a single length parameter is used to compensate for the mesh pathology. As masonry component consists of mortar joints and units, each element of the

mesh should encompass some part of the mortar and block to provide physically consistent results.

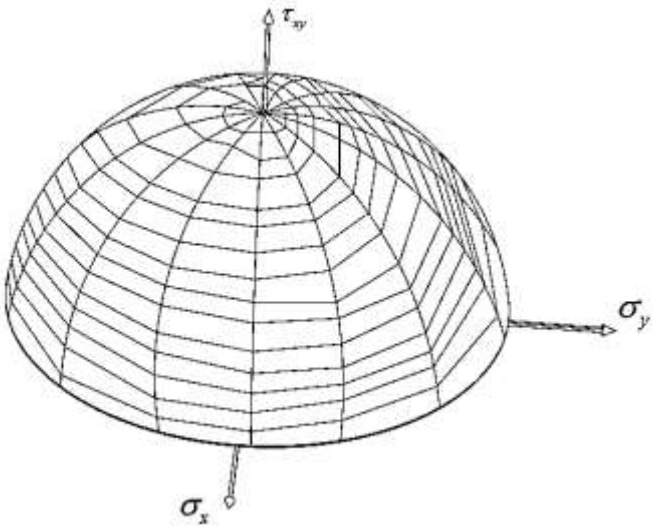

Figure 5. Hill type yield surface

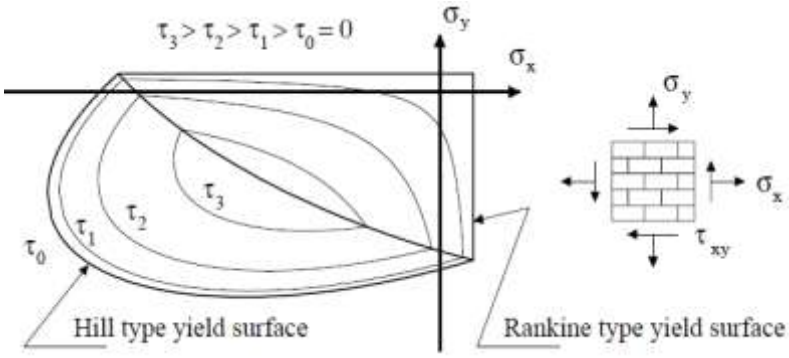

Figure 6. Composite yield surface with iso-shear stress lines [31]

Masonry was modelled using four node bilinear reduced integration plane stress continuum elements (CPS4R). Due to selected reduced integration, the hourglass control was activated which enabled the hourglass energy that lies within the 10% of the internal energy of the system. Effective thickness of the hollow masonry was 31.5 mm and that of the grouted masonry was 95mm. The properties of hollow masonry are listed in Table 2. By conducting mesh convergence analyses, it has been found that a mesh dimension of 110mm×95mm is optimal; this size represents half size block with head and bed joints.

3.2 Grouted cores

This paper treats the grouted cores (combination of masonry block shells, mortar and grout) as an anisotropic continuum. Hence, they are treated with similar material properties as that for the hollow masonry detailed in Section 3.1). However their numerical values are different from that of the hollow masonry. The parameters obtained from material testing are presented in Table 3. For the grouted element the mesh dimension of 95mm×95mm was selected to represent a grout effective width and one block height with mortar.

3.3 Reinforcement

Reinforcement bars were modelled using wire feature associated with truss element. A limited compression of 1*MPa* was allowed in the steel reinforcement since the reinforcement located in the grout would not resist compression load at the absence of lateral ties. These truss elements were embedded in CPS4R element representing masonry grout. Truss elements were two node linear elements denoted by 'T2D2' in ABAQUS. Figure shows the typical truss element which represents 1N12 reinforcement embedded in the grout.

The way in which steel embedded elements act with host CPS4R element (grout) is briefly explained. In Fig. 7, steel embedded element is shown using node numbers 1,2,3,4 and5 whereas the host grout element is shown by elements X,Y and Z (CPS4R). Element X is defined by nodes A, B, G and H, element Y is defined by nodes B, C, F and G and element Z is defined by nodes C, D, E and F. The embedded steel wire element node 1 lies inside host element X. All degree of freedom of node 1 is constraint with node A, B, G and H with an appropriate weight factor.

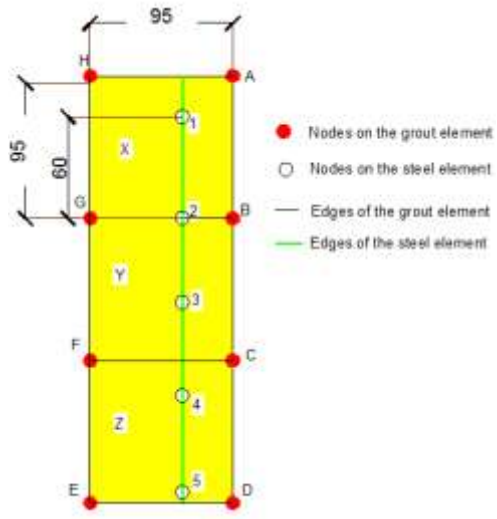

Figure 7. Embedded steel element

This weight factors is determined by geometric location of '1' in the element-X. Since node-2 is located on edge B-G, its degree of freedom is restrained with B and G with an appropriate weight factors. Simultaneously node 3, 4 and 5 are restrained with element Y and Z, respectively.

Since the compression stress in steel is limited to just 10MPa (due to lack of lateral steels), only tension was active on the steel reinforcement. A VUMAT subroutine written in FORTRAN was adapted for this purpose [21]. Nine parameters were used to represent the steel reinforcement material model. Fig. 8 shows the stress-strain curve of steel reinforcing bars.

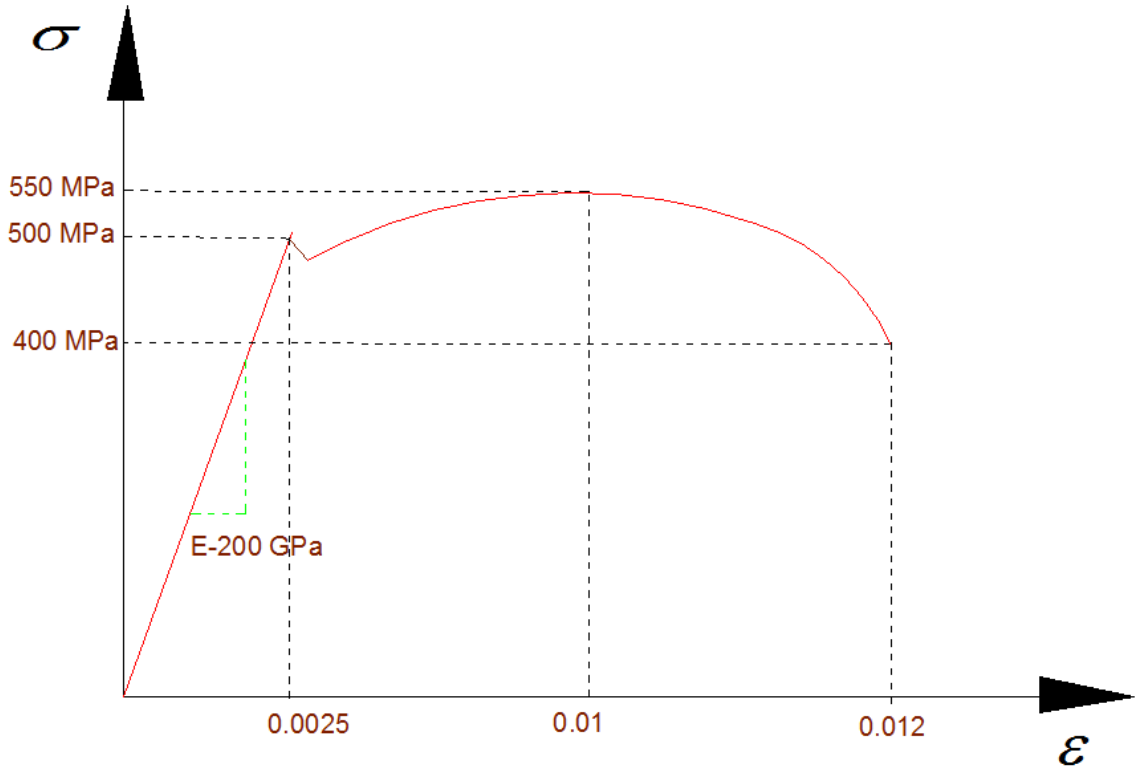

Figure 8. Steel stress-strain response

3.4 Explicit analysis

Explicit analysis method reported in ABAQUS[26]was adopted for the current problem because it deals with highly non-linear materials degradation process and complex mechanism of failure. Material degradation often leads to severe convergence difficulties in standard implicit analysis programs, but ABAQUS/Explicit method is capable of handling such degradation adequately. More details about the explicit formulation for reinforced masonry can be found elsewhere [32].

4 Calibration and Validation

The conditionally stable explicit was calibrated with material, geometric (mesh) and time-step parameters such that the kinetic energy of the system cannot exceed 10% of the internal energy of the total system. The geometric details and meshing are shown in Fig. 9. The corresponding energy plots are shown in Fig. 10(a) and Fig. 10(b).

It is clear from Fig. 10(b) that whenever the kinetic energy is suddenly increased, a drop of load is exhibited, which indicates the formation of crack. At a displacement near 8 mm considerable amount of kinetic energy dissipation was noticed with corresponding drops in load which indicates the formation of major cracks prior to termination of the analysis. It can be seen from Fig. 10(b) that the kinetic energy was kept very low relative to the internal energy. It can therefore be seen that the inertia effect was successfully minimised hence the model could exhibit closer behaviour to that of the statically loaded experiment walls. For all analysed walls the kinetic energy was ensured within 10% of the internal energy.

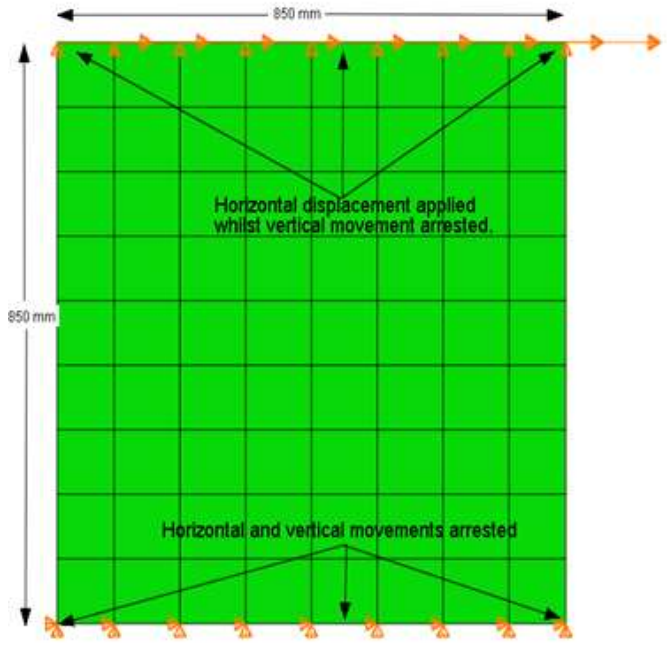

Figure 9. Wall details for viability of explicit analysis

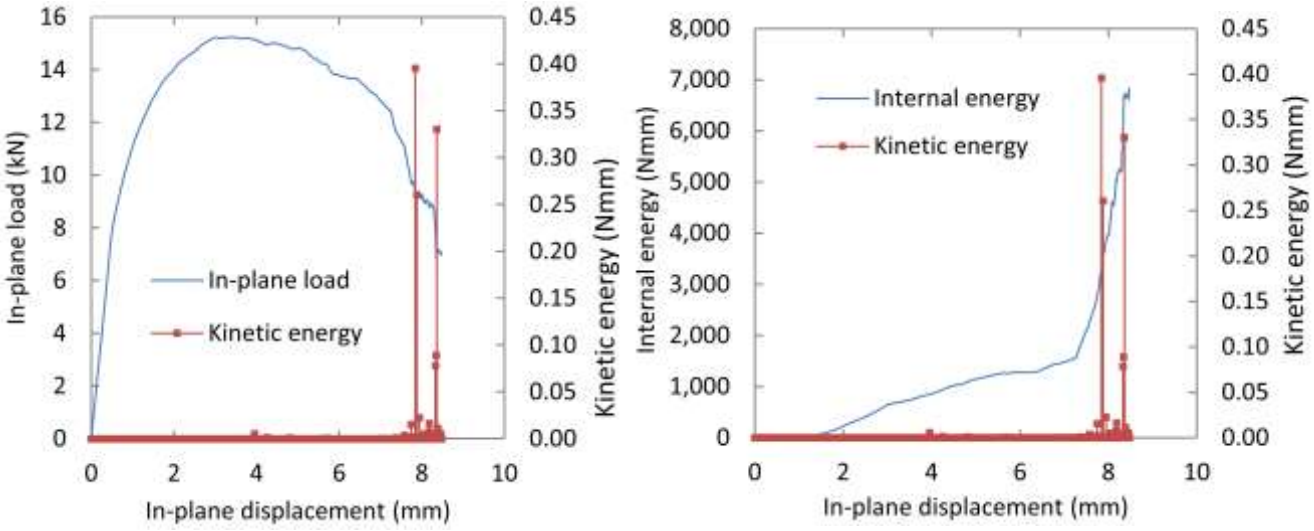

a) Kinetic energy and load response

b) Kinetic energy and internal energy

Figure 10. Kinetic energy versus displacement

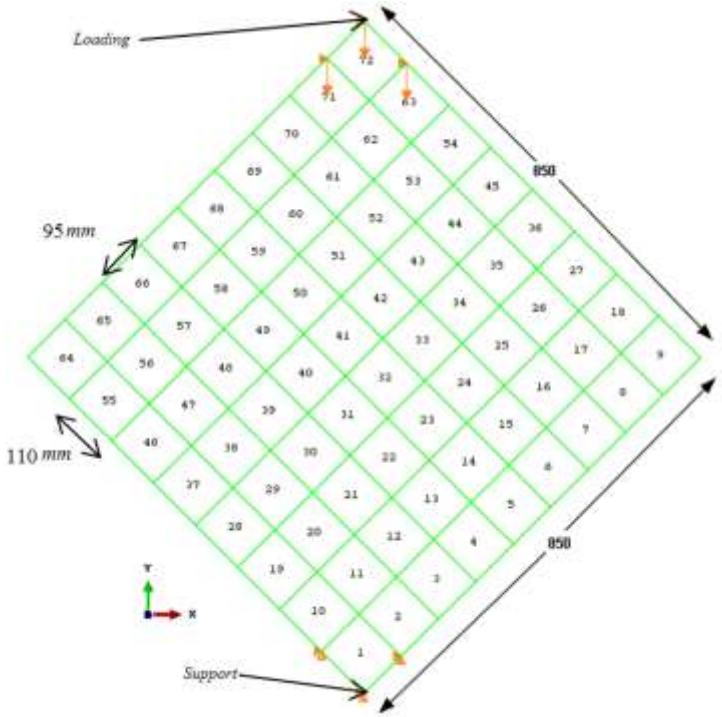

Figure 11. Mesh arrangement of the UCM panels

Table 2.Material properties for masonry

No.	Details	Parameters	Values	Source/details.
1	Tensile strength parallel to bed joints	$f_{tp}(Nmm^{-2})$	0.5	Determined from f_{tp}/f_{tn} ratio [31]
2	Fracture energy parallel to bed joints	$G_{tp}(Nmm/mm^2)$	0.65	Determined from G_{ftp}/G_{ftn} ratio [31]
3	Tensile strength normal to bed joints	$f_{tn}(Nmm^{-2})$	0.27	Assumed equal to f_{mt}/1.5 [33]. f_{mt}=0.4 MPa (ref. Table 1)
4	Fracture energy normal to bed joints	$G_{tn}(Nmm/mm^2)$	0.3	Determined from test results.
5	Shear stress contribution factor to the tension failure	α	1.25	Recommended [31, 34]
6	Mathematical variable for plastic flow of masonry	α_g	1	Recommended [31]
7	Compressive strength parallel to bed joints	$f_{hmc\|\|}(Nmm^{-2})$	2.95	Determined from f_{cp}/f_{cn} ratio [31]
8	Energy for compression failure parallel to bed joints	$G_{hmc\|\|}(Nmm/mm^2)$	1	Determined from G_{fcp}/G_{fcn} ratio [31]
9	Compressive strength normal to bed joint	$f_{hmc\perp}(Nmm^{-2})$	9.2	Determined from test results (Ref. Table-1).
10	Energy for compression failure normal to bed joints	$G_{hmc\perp}(Nmm/mm^2)$	6	Determined from test results.
11	Biaxial compressive strength factor	β	-1.17	Recommended [31]
12	Shear stress contribution factor to compression failure	γ	4	Recommended [31, 35]
13	Strain at compression failure	ε_p	0.0025	Obtained from test results.
14	Characteristic length of critical elements	h (mm)	102	Determined using equation given in Lourenço[31]
15	Young's Modulus of masonry parallel to bed joints	$E_{hmc\|\|}(MPa)$	800	Determined from E_p/E_n ratio [21, 31]
16	Young's Modulus of masonry normal to bed joints	$E_{hmc\perp}(MPa)$	2155	Obtained from test results.
17	Young's Modulus of masonry along thickness direction	$E_z(MPa)$	0.001	Assumed. Very lower value was considered.
18	Poisson's Ratio of masonry parallel to bed joints	υ_p	0.2	Recommended [21, 31]
19	Poisson's Ratio of masonry normal to bed joints	υ_n	0.2	Recommended [21, 31]
20	Poisson's Ratio of masonry along thickness direction	υ_z	$1e^{-7}$	Assumed. A very lower value was considered.
21	Shear Modulus of masonry of masonry	$G(MPa)$	780	Determined using equation given in Lourenço[31]

The actual meshing used for UCM is shown in Fig. 11. In which, the bottom shoe is denoted as '*Support'* and Loading shoe is denoted as '*Loading'*. In the *Support* all vertical and horizontal displacement degrees of freedom (DOF) were arrested whereas in the *Loading* the vertical DOF was released whilst arresting horizontal movement. The loading was applied as same as experimental at a rate of 1mm/min. The material calibration was carried out for UCM panels.

The calibrated parameters for UCM panels are shown in Table 2. The reasoning behind the selection of each value is stated in the table. For the calibration, the range of values obtained from the material tests was considered.For example, the tensile strength normal to bed joint (f_{tn})value was obtained by dividing the flexural tensile strength by 1.5. The flexural tensile test results were in between 0.32*MPa*and 0.62*MPa*. It allowed fluctuation of f_{tn} in between 0.21*MPa*and 0.41*MPa*. For f_{tn}, the calibrated value of 0.27 *MPa* was found as optimum. Similarly, other parameters were calibrated.

For the grouted cores the same 21 parameters were calibrated with new values. Those new values are reported in Table 3. Since there is no standard direct/indirect tests procedure exist to evaluate grouted masonry tensile test slightly higher value than that of UCM panels were considered. $f_{hmc\perp}$ and $G_{hmc\perp}$ values were obtained from tested grouted prisms. The shear stress contribution factor to compressive failure γ was reduced to 2, considering the grout pure shear strength (τ_u) would be higher. The value of γ was determined using Eq.2 in which $f_{hmc\|}$ and $f_{hmc\perp}$ indicate masonry compressive strength parallel to bed joint and perpendicular to bed joint, respectively.

$$\gamma = \frac{f_{hmc\perp} f_{hmc\|}}{\tau_u^2} \tag{2}$$

The average strain at compression failure (ε_p) of 0.001 was obtained from experimental test results. The modulus of elasticity perpendicular to bed joint ($E_{hmc\perp}$) was obtained through test results and perpendicular to bed joint ($E_{hmc\|}$) was found using the similar ratio as of UCM, considering similar anisotropic nature exist in the grouted masonry. For the Poisson's ratios a value of 0.22 was considered[21].

Table 3. Material properties for grout

No.	Details	Parameters	Value for grout
1	Tensile strength parallel to bed joints	$f_{tp}(Nmm^{-2})$	0.55
2	Fracture energy parallel to bed joints	$G_{tp}(Nmm/mm^2)$	1
3	Tensile strength normal to bed joints	$f_{tn}(Nmm^{-2})$	0.32
4	Fracture energy normal to bed joints	$G_{tn}(Nmm/mm^2)$	0.55
5	Shear stress contribution factor to the tension failure	α	1.25
6	Mathematical variable for plastic flow of masonry	α_g	1
7	Compressive strength parallel to bed joints	$f_{gmc\parallel}(Nmm^{-2})$	2.95
8	Energy for compression failure parallel to bed joints	$G_{gmc\parallel}(Nmm/mm^2)$	0.8
9	Compressive strength normal to bed joint	$f_{gmc\perp}(Nmm^{-2})$	8.7
10	Energy for compression failure normal to bed joints	$G_{gmc\perp}(Nmm/mm^2)$	2.5
11	Biaxial compressive strength factor	β	-1.17
12	Shear stress contribution factor to compression failure	γ	2
13	Strain at compression failure	ε_p	0.001
14	Characteristic length of critical elements	h (mm)	95
15	Young's Modulus of masonry parallel to bed joints	$E_{gmc\parallel}(MPa)$	5300
16	Young's Modulus of masonry normal to bed joints	$E_{gmc\perp}(MPa)$	14500
17	Young's Modulus of masonry along thickness direction	$E_z(MPa)$	0.0001
18	Poisson's Ratio of masonry parallel to bed joints	υ_p	0.22
19	Poisson's Ratio of masonry normal to bed joints	υ_n	0.22
20	Poisson's Ratio of masonry along thickness direction	υ_z	$1e^{-7}$
21	Shear Modulus of masonry of masonry	$G(MPa)$	3500

The final stress responses of two UCM panels are shown in Fig. 12. Reasonably good agreements of predicting peak strength and failure displacement were obtained. The experimental failure diagonal displacements were 4.2 and 4.3mm whereas the FE model failed at 4.3 mm with reasonable prediction of peak shear strength.

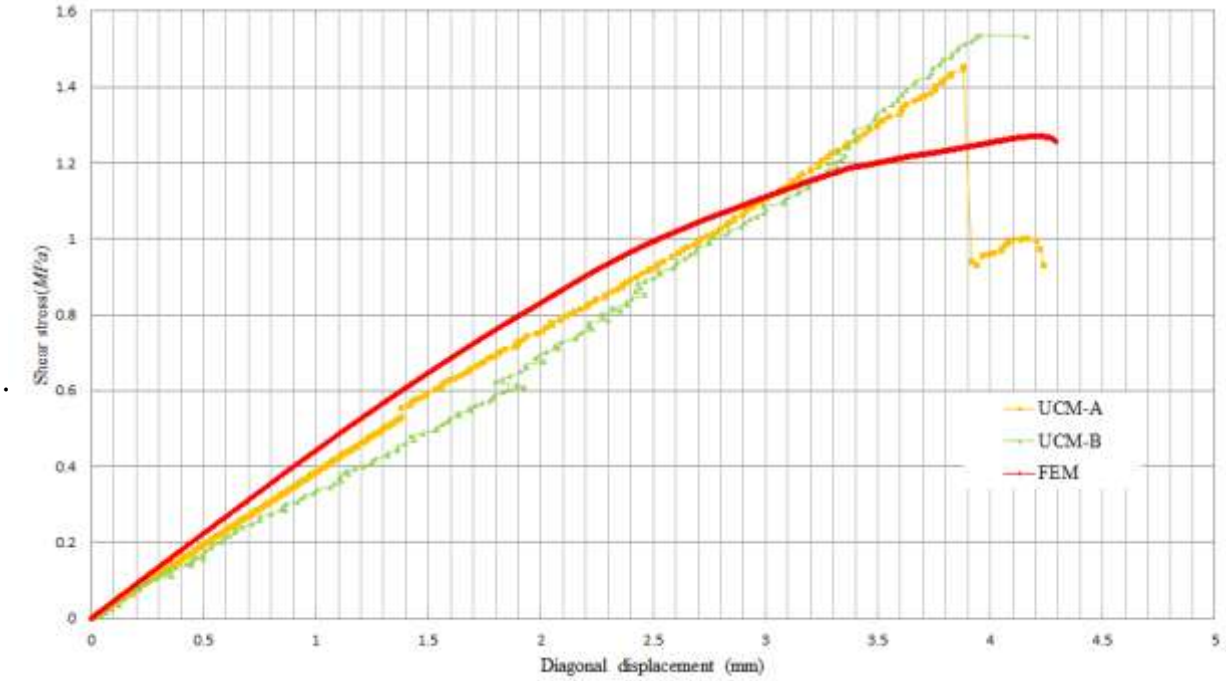

Figure 12. Shear stress versus diagonal displacement of UCM panels.

In the experiment of the two CM panels failed at a diagonal displacement of 5.2mm and 5.3mm respectively, which compare well with the 5.4mm predicted by the FE model. Similarly, the panels failed at 1.54 *MPa*and 1.66 *MPa* respectively, which compare quite well with the peak shear stress prediction of FE model (1.57*MPa).* Therefore, it can be said that the FE model with the calibrated parameters can successfully predict the behaviour of the UCM and CM walls in terms of shear stress response and diagonal displacement.

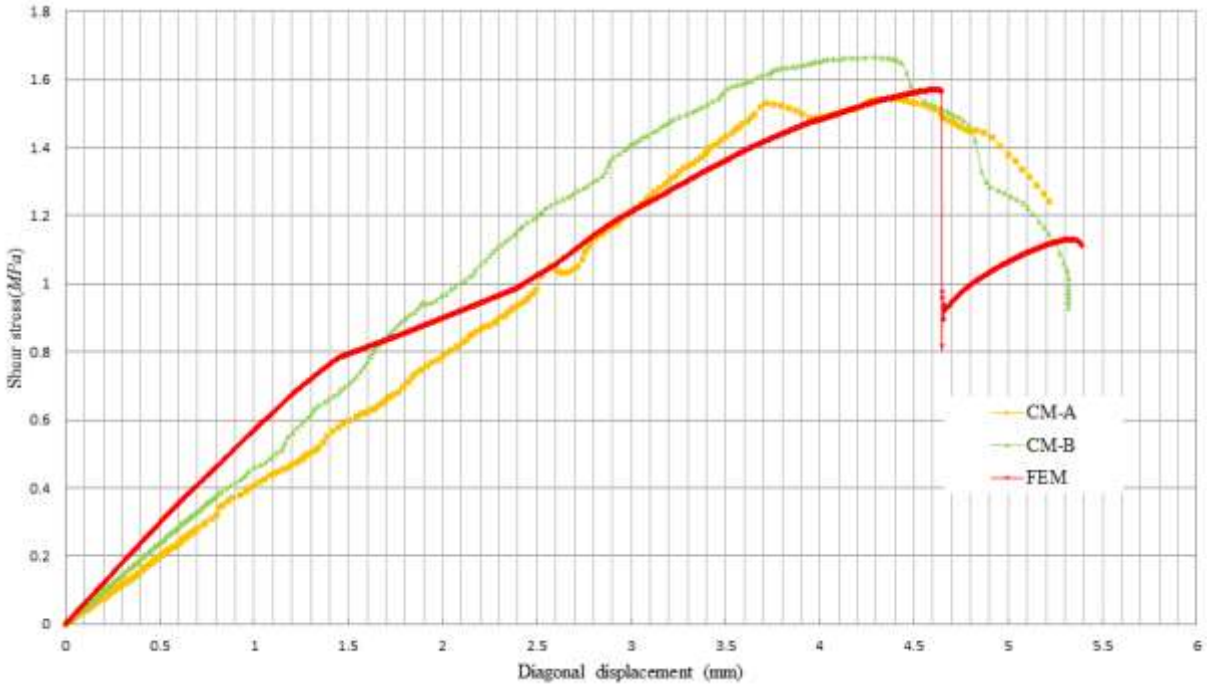

Figure 13. Shear stress versus diagonal displacement of CM panels

Further to shear stress-displacement validation, the failure mode was also validated. ABAQUS graphic user interface could not show cracks explicitly. Therefore, logarithmic strain plot was chosen as representative of the cracks. Fig. 14(a) shows vector plots of the logarithmic principal strains of the panel at failure whereas Fig. 14(b) shows the failure of the UCM experimental panel. The general diagonal splitting failure was experienced in the UCM panels. Simulated FE model exhibited a principal tensile logarithmic strain of 660μ and principal compressive logarithmic strain of -1,400μ at a diagonal displacement of 1mm. With further loading the failure occurred at a 4.3 mm diagonal displacement at which the principal tensile logarithmic strain was 18,000$\mu$and principal compressive logarithmic strain was -6,600μ. The compressive strain has enhanced by 4.7 times while tensile strain enhanced by 27 times which indicates the diagonal tensile split of the panel.

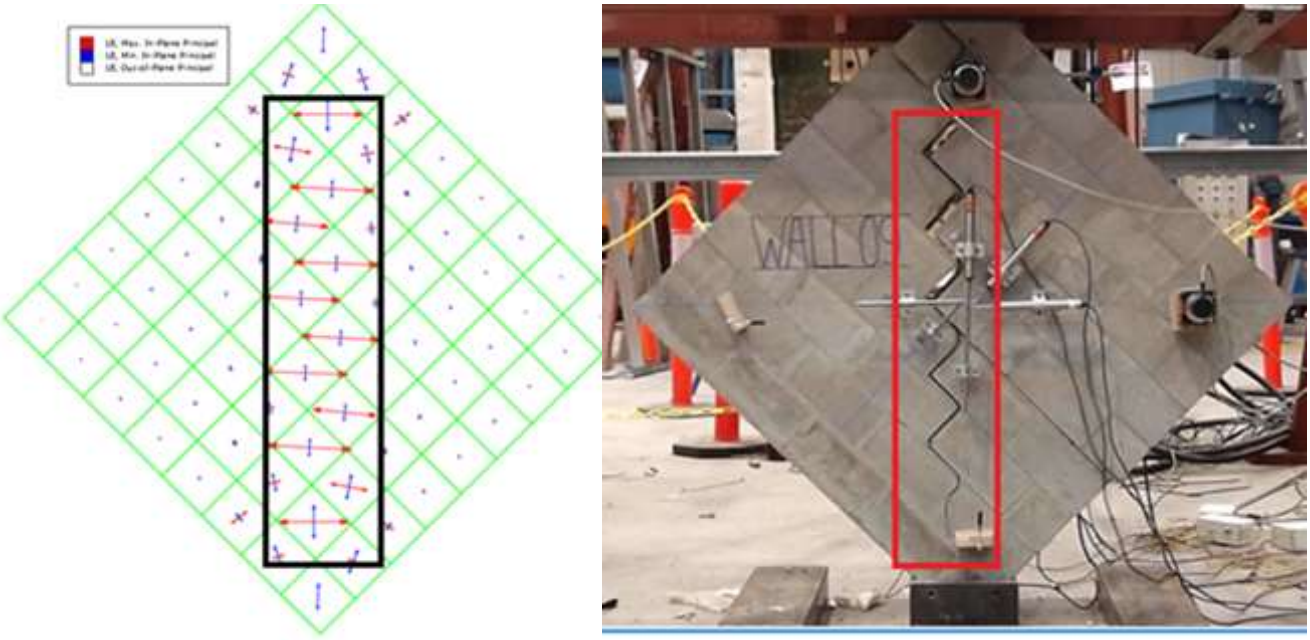

a) At displacement of 5.4 mm (failure).

b) At failure.

Figure 14. Failure of UCM panels

Figs. 15(a) and 15(b) show the FE results of logarithmic principal strains of the CM panel at failure and the typical failure of the experimental panel, respectively. At 1mm of diagonal displacement, the FE model exhibited principal tensile logarithmic strain of 1,500μ and principal compressive logarithmic strain of -1,200μ in which the panel behaved elastically. At the failure displacement of 5.4mm, the principal tensile logarithmic strain was 42,000μ and principal compressive logarithmic strain was -28,700μ. Very high principal tensile strain indicates cracking at those points.

At the peak load of both URM and CM panels, the principal tensile logarithmic strains were between 17,900-18,000μ. With further loading URM panel lost its ability to withstand any further loading and failed through diagonal splitting. However, the CM panel withstood further loading as shown in Fig. 13. It is also worth to mention that, in Fig. 15(a) very high compressive strains exhibited at bottom support level where the experimental panels exhibited cracking in the blocks either near the loading shoe/ support shoe, which further enhances the confidence of the FE model as a good predictor of the complex modes of failure of the diagonally loaded unconfined and confined masonry panels.

FE model prediction of the shear strength of panels (reported in section 5) were used to evaluate the existing in-plane shear expressions.

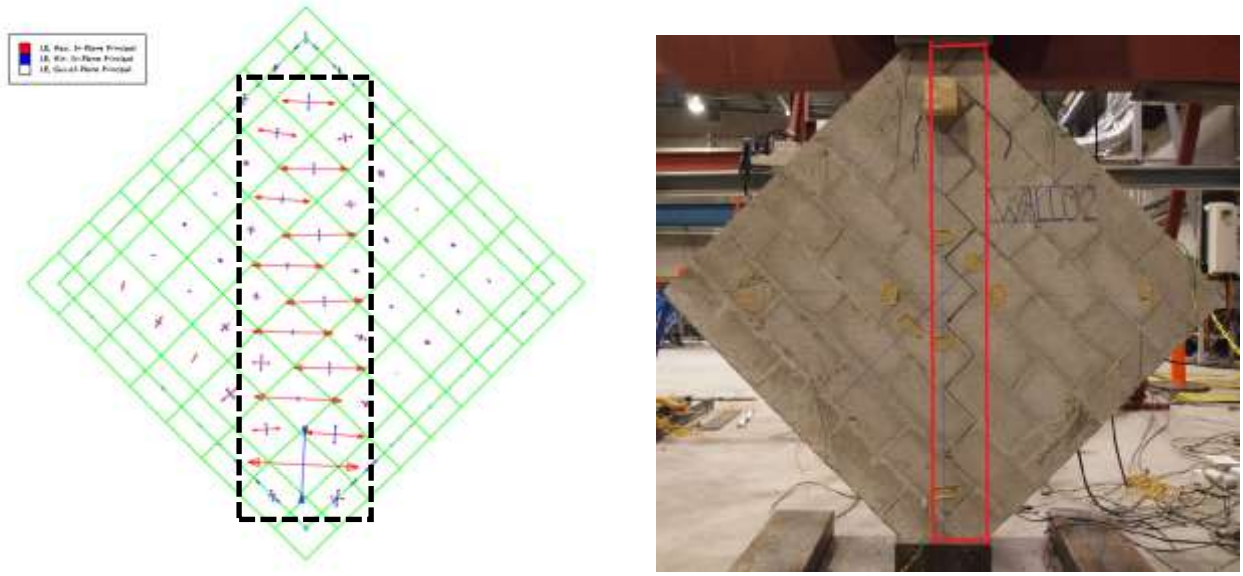

a) Principal logarithmic strain at (failure).

b) At failure.

Figure 15. Failure of CM panels

5 Shear strength

Six empirical shear strength expressions for reinforced masonry considered in the study,:(1) MSJC(2008)[15], (2) AS3700(2011) [16], (3) CSA:S304.1-04 (2004)[17], (4) NZS-4230 (2004)[18], (5) Matsumura(1988)[20] and (6) Shing et al.[19]. These empirical formulae, except the one in AS3700(2011) and Matsumura(1988), were initially derived from fully grouted masonry shear walls. For the partially grouted walls these formulae were treated with either, net area (A_n) instead of gross area (A_g) in Equations.3,5,6 and 8 or coefficients to account partially grouting in Equations.4 and 7. Two types of net area were considered, either including or excluding the grouted area. NZS-4230 (2004) accounts only the face-shell bedded area thereby fully neglecting its grouted cells to the shear strength. This criterion was selected to satisfy shear flow continuity requirements and assuming a possibility of vertical shear failure of continuous ungrouted cells.

Table 4. Inplane shear equations

Name (Eq No.)	**Masonry (V_m)**	**Vertical load(V_p)**	**Vertical steel (V_s)**	**Horizontal steel(V_s)**
AS 3700 [1]	$f_{vr}=\left(1.5-0.5\frac{H}{L}\right)A_n$	-	$0.8 f_y A_s$	
CSA (2004) [2]	$\left[0.16\left(2-\frac{M_f}{V_f d_v}\right)\sqrt{f_m^{'}}\right]\gamma_g b_w d$	$0.25P\gamma_g$	-	$0.6 f_{yh} A_{sh}\frac{d}{s_h}$
MSJC(2008) [3]	$\left[0.166\left(2-0.875\frac{M_f}{V_f d_v}\right)\sqrt{f_m^{'}}\right]A_n$	$0.25P$	-	$0.5 f_{yh} A_{sh}\frac{d_v}{s_h}$
NZS-4230 (2004) [4]	$0.42\left[4-1.75\frac{H_e}{L}\right]v_{bm} b_w d$	$0.9P\tan\alpha$	$33\frac{A_{sv} f_{yv}}{300}v_{bm}$	$0.8 f_{yh} A_{sh}\frac{d}{s_h}$
Matsumura (1988) [5]	$k_u k_p\left(\frac{0.76}{\frac{H_w}{L_w}+0.7}+0.012\right)\times\sqrt{f_m^{'}}\times 0.875A_n$	$0.175P$	k_p	$0.1575\gamma\delta\sqrt{\rho_h f_{yh} f_m^{'}}A_n$
Shing et al. (1990) [6]	$0.166A_n\sqrt{f_m^{'}}$	$0.00015P\sqrt{f_m^{'}}$	$0.00015\rho_v f_{yv} A_n\sqrt{f_m^{'}}$	$(n-2) f_{yh} A_{sh}$

AS3700(2011) expression shown in Eq 3 accounts for the aspect ratio in the masonry term while neglecting the strength of the masonry. Significant amount (80%) of yield strength of reinforcement (the minimum of vertical or horizontal) was accounted although the contribution of reinforcement to in-plane shear capacity is position dependent. The V_m term of this equation does not seem to be derived from any fundamental mechanisms. The areas of reinforcement terms consider the lesser of either the total horizontal reinforcement or the vertical reinforcement indicating a same level contribution from both vertical and horizontal reinforcements.

$$V_n = \left(1.5 - 0.5\frac{H}{L}\right)A_n + 0.8 f_y A_s \quad (3)$$

CSA (2004) and NZS-42030 (2004) also contained an aspect ratio factor in the masonry term. NZS-42030 (2004) accounted the effect of vertical reinforcement and limited the contribution of vertical load to $0.1f_mA_g$. More details of this equation can be found in Voon and Ingham (2007)[36].

$$V_n = \left[0.16\left(2 - \frac{M_f}{V_f d_v}\right)\sqrt{f_m^{'}}\right]\gamma_g b_w d + 0.25P\gamma_g + 0.6 f_{yh}A_{sh}\frac{d}{s_h} \quad (4)$$

$$V_n = 0.42\left[4 - 1.75\frac{H_e}{L}\right]v_{bm}b_w d + 0.9P\tan\alpha + 33\frac{A_{sv}f_{yv}}{300}v_{bm} + 0.8 f_{yh}A_{sh}\frac{d}{s_h} \quad (5)$$

The MSJC(2008) contains V_m term similar to that of the CSA (2004). MSJC(2008) does not address the masonry shear strength within the plastic hinge regions for masonry structures that are subjected to inelastic response. The maximum shear strength was limited to $0.5A_n\sqrt{f_m^{'}}$ and $0.33A_n\sqrt{f_m^{'}}$ for $M_f / V_f d_v \le 0.25$ and $M_f / V_f d_v \ge 1$, respectively. A straight line interpolation is allowed for $M_f / V_f d_v$ values between 0.25 and 1.00. $0.5A_n\sqrt{f_m^{'}}$ and $0.33A_n\sqrt{f_m^{'}}$ for $M_f / V_f d_v \le 0.25$ and $M_f / V_f d_v \ge 1$, respectively. A straight line interpolation is allowed for $M_f / V_f d_v$ values in between 0.25 and 1.00.

$$V_n = \left[0.166\left(2 - 0.875\frac{M_f}{V_f d_v}\right)\sqrt{f_m^{'}}\right]A_n + 0.25P + 0.5 f_{yh}A_{sh}\frac{d_v}{s_h} \quad (6)$$

Matsumura(1988) developed Eq. 7 based on own test results and other tested walls in Japan. A regression analysis was used to identify the parameters represented in Eq.6; where k_u accounts partial grout, k_p accounts vertical reinforcement, δ accounts type of loading and γ accounts the action to confine grout. This expression also accounts the effect of aspect ratio. Only the vertical reinforcement provided by the edge bars is considered.

$$V_n = k_u k_p\left(\frac{0.76}{\frac{H_w}{L_w} + 0.7} + 0.012\right) \times \sqrt{f_m^{'}} \times 0.875A_n + 0.175P + 0.1575\gamma\delta\sqrt{\rho_h f_{yh} f_m^{'}}A_n \quad (7)$$

Shing et al. (1990) developed the equation using regression analysis (Eq 8). This equation accounts for the contribution from a masonry component, an axial load component and a vertical and shear reinforcement components. Unlike the equation of Matsumura(1988), all vertical reinforcement is considered. The ineffectiveness of the top and the bottom layers of horizontal shear reinforcement embedded in the loading and support grouts due to insufficient embedment length to develop their yield capacity following the diagonal shear cracking is accounted for in this equation.

$$V_n = \left(0.166A_n + 0.00015P\right)\sqrt{f_m^{'}} + 0.00015\rho_v f_{yv} A_n \sqrt{f_m^{'}} + \left(n-2\right) f_{yh} A_{sh} \qquad (8)$$

These empirical formulas are derived for the walls that are loaded in the horizontal direction whilst the bottom masonry layer is fully restrained (refer Figure). The masonry panels loaded in the diagonal direction cannot be directly evaluated using these formulas. The validated FE model using diagonally loaded panel test results was used for the analysis of a 850mm square cantilever reinforced grout confined masonry panel; its in-plane shear capacity was evaluated (V_{FE}). The ratio of empirical formula prediction (V_n) with FE model prediction (V_{FE}) for different equations is shown in Fig. 16. A value of Vn/V_{FE} above unity is unconservative. A value of Vn/V_{FE} equals to one indicates exact prediction of in-plane shear capacity; less than unity yield conservative prediction of empirical formulae.

For the calculation of V_n no horizontal reinforcements were considered since there was no effective horizontal reinforcement. Two horizontal reinforcements (1N12 reinforcement in each grout) were placed in the top and bottom grout which are considered ineffective.

It can be seen from Fig. 16, the MSJC (2008) provides the best performing equation. The in-plane shear capacity of UCM predicted by MSJC (2008) was exactly similar to FE model results while the in-plane shear capacity of CM panel was predicted 8 % lower, which is conservative. The MSJC (2008) predictions are thus conservative. Similarly, NZS 4230(2004) also predicted the FE model results for UCM. Therefore the MSJC (2008) and NZS 4230(2004) seems to be successfully predicting the in-plane shear capacity of small masonry panels.

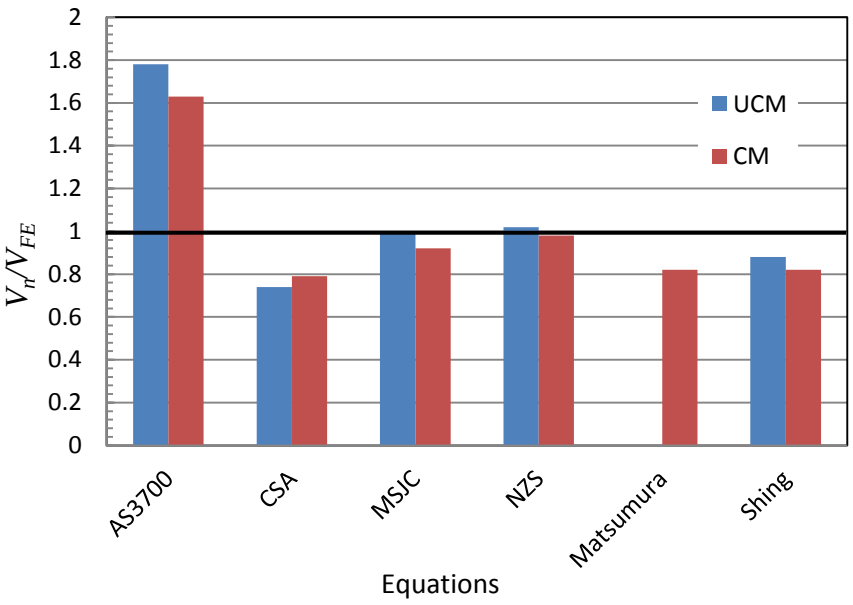

Figure 16.Vn/V_{FE} versus equations

The Australian Masonry standard is highly unconservative, consistent with the conclusions made by Shrive[4], Dhanasekar[22] and Mosele[23]. Even though no provisions have been made in the standard for the ineffective reinforcement the empirical formula of in-plane shear capacity was considered without any horizontal reinforcement terms. In the absence of accounting ineffective reinforcement, it over predicts the capacity by 70%.

Since the ineffective reinforcement was not considered in the evaluation of capacity using existing in-plane shear expressions, it is important to examine the tensile stress level induced in the ineffective reinforcements. Fig. 17 shows the tensile stress of the reinforcement (N12) located in aspect ratio (λ) of 1 panels along its length at two different stages; i) at the peak load stage of the panel and ii) at the ultimate failure load stage of the panel. Two ineffective locations of the reinforcements are considered; i) *Loading*- where reinforcement located in the grout located near loading and ii) *Support*- where reinforcement located in the base grout. The graphs are denoted by its loading stage followed by its location (for example, tensile stress of reinforcement located near loading at peak load is denoted as “Peak_Loading”).

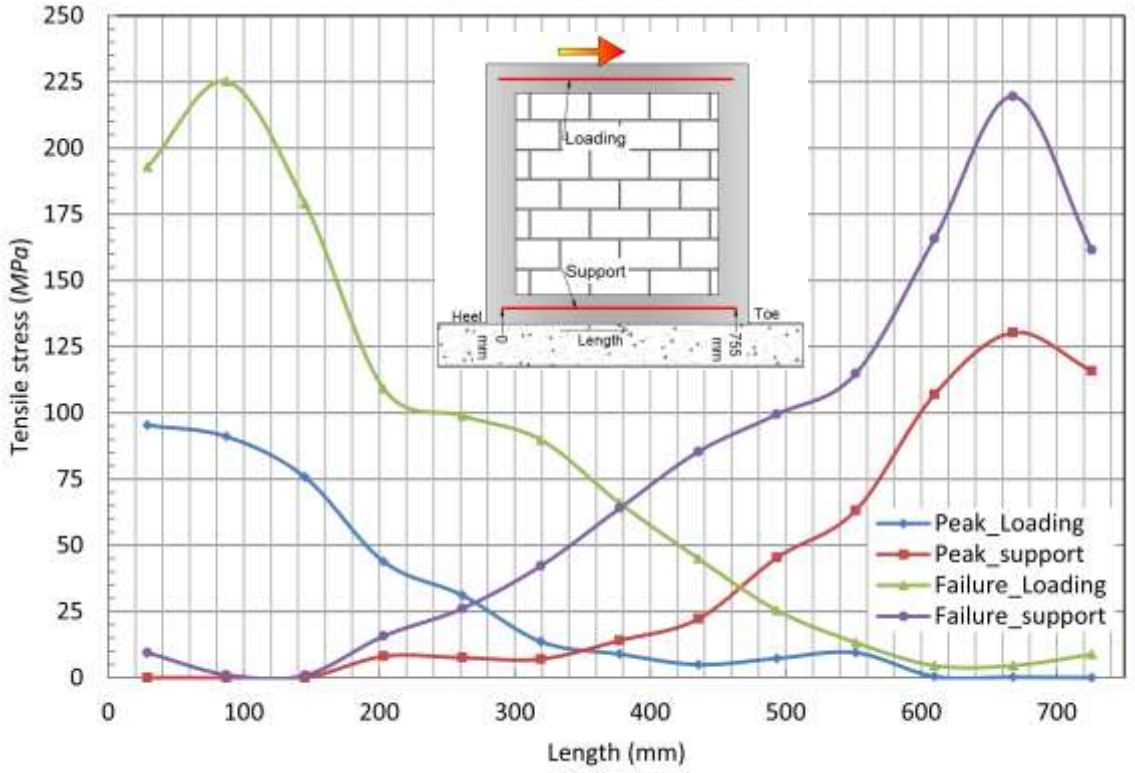

Figure 17. Tensile stress on the reinforcements (λ=1.0)

It is noted that there were no yielding reported in the reinforcement (yield strength-500*MPa*). The *Loading* reinforcement is active near the heel side whereas the *Support* reinforcement is active near the toe side. It also should be noted that the horizontal reinforcements appeared to be more effective at the failure compared to the peak load which probably reduce the brittle failure of the wall. At the peak load only 20% of the yield strength was experienced by the reinforcement.

Furthermore analysis was conducted on λ of 0.8 panels and 0.65 panels to identify tensile stress on the reinforcement. Since the reinforcement contribution to enhance in-plane shear capacity was our major concern, only the tensile stresses of the reinforcement at the peak load capacity of the panels are reported in Fig. 18. The graphs are denoted by its reinforcement location followed by its panel aspect ratio (for example, an aspect ratio of 0.8 panel's tensile stress of reinforcement located near loading is denoted as "Loading_λ=0.8"). There was no yielding found at any stages of peak load capacity of the panel. Therefore, it is conservative to disregard any contribution from these ineffective reinforcements for the calculation of in-plane shear capacity.

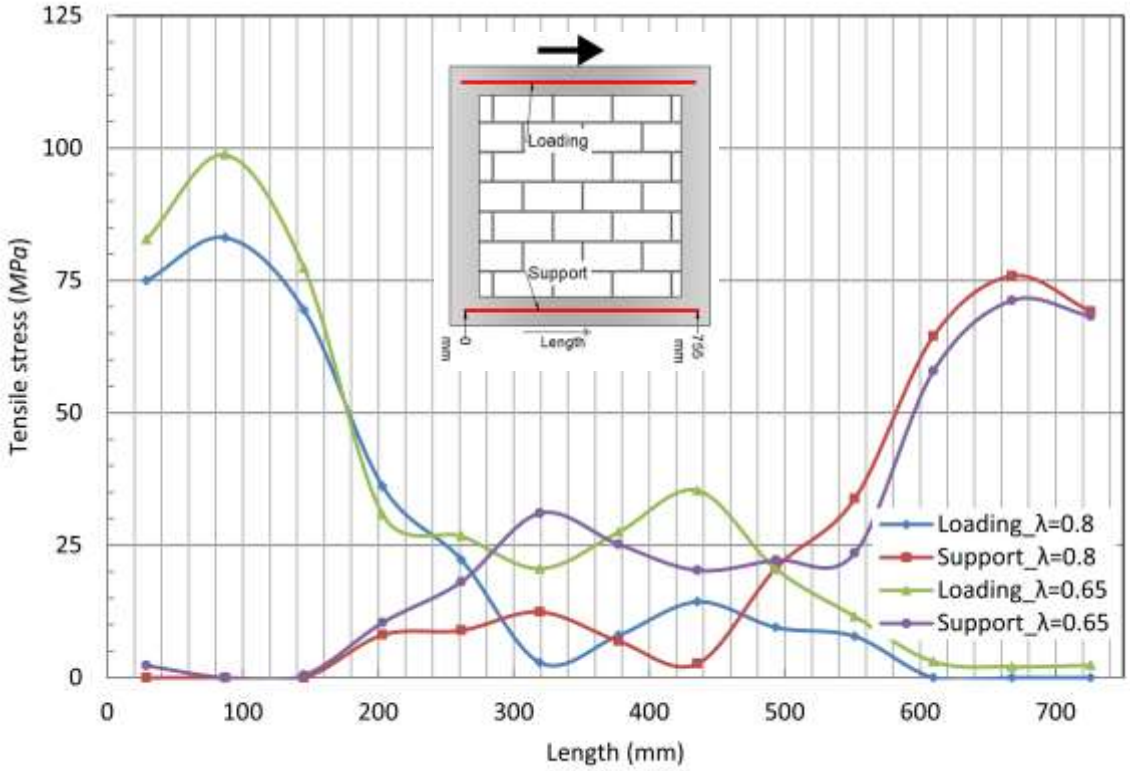

Figure 18. Tensile stress on the reinforcements (λ=0.8 & 0.65)

6 Conclusions

A macro FE model in explicit framework developed for wide spaced reinforced masonry was adapted to simulate the behaviour of diagonally loaded unreinforced unconfined masonry and reinforced grout confined masonry panels. It is shown that the FE model is effective in determining the shear strength, failure mode and post-peak deformation characteristics of the masonry panels. Two sets of tests were carried out; i) characterisation of materials and ii) diagonal test on masonry panels. 55 small specimens and masonry sub assemblages were tested to characterise the material and 4 masonry panels-consisting two panels each of unreinforced masonry and confined masonry configurations were tested. Complete set of material properties that enabled the prediction of the response of masonry panel have been provided in this paper.

The following conclusions were drawn from the study.

- The adapted explicit macro FE modelling approach predicts the in-plane shear behaviour of the diagonally loaded panels, which compared well with the experimental datasets. Hence the FE model provides encouragement for further studies on the post peak behaviour of the masonry shear walls.
- Predictions made by FE models were compared with in-plane shear empirical expressions published in various national standards and some selected literature. The predictions of the MSJC (2008) and the NZS4230(2004) are found conservative and very close to the predictions of the FE model.
- Australian Masonry Standard (AS3700-2011) in-plane shear formula overestimates the capacity by 70%. This formula needs an urgent review.

Acknowledgements

The authors wish to acknowledge the donation of half scale blocks for the experiment by Mr.David Stubbs, Director of the Canada Masonry Design Centre. QUT scholarship and fee waiver to the first author are also thankfully acknowledged. The experiments were supported by the Concrete Masonry Association of Australia (CMAA).

Notation

A_g - Gross sectional area (mm^2);

A_n - Net area (mm^2);

A_s - Area of reinforcement (mm^2);

A_{sh} - Area of horizontal reinforcement (mm^2);

A_{sv} - Area of vertical reinforcement (mm^2);

b-Width of the block/wall (mm);

b_w- Effective width of the wall (mm);

d- Distance from extreme compression fibre to centre of longitudinal tension reinforcement or 0.8 L for walls (mm);

d_v - Effective depth for shear calculations should be greater than $0.8L$ (m);

$f_{hmc\perp} / f_m$ -Mean compressive strength of hollow masonry perpendicular to bed joint (*MPa*);

$f_m^{'}$ - Characteristic compressive strength of masonry (*MPa*);

f_{yh} -Yield strength of horizontal reinforcement (*MPa*);

f_{yv} -Yield strength of vertical reinforcement (*MPa*);

H_e -Effective wall height (m);

H -Wall height (m);

k_p -Coefficient of the effect of flexural reinforcement;

k_u -Reduction factor;

L -Wall length (m);

$M_f / V_f d_v$ - Aspect ratio;

n- Number of horizontal grouts;

P- Pre compression load (kN);

s_h - Spacing of horizontal shear reinforcement.

v_{bm}- basic shear strength provided by masonry (*MPa*);

V_n- In-plane shear capacity of the wall (kN);

λ- Aspect ratio;

γ -Factor concerning the type of grouting;

δ -Factor concerning the loading method;

References

[1] Tena-Colunga A, Juárez-Ángeles A, Salinas-Vallejo VH. Cyclic behavior of combined and confined masonry walls. Engineering Structures. 2009;31(1):240-59.
[2] Ruiz-García J, Negrete M. Drift-based fragility assessment of confined masonry walls in seismic zones. Engineering Structures. 2009;31(1):170-81.
[3] Dhanasekar M, Haider W. Effect of spacing of reinforcement on the behaviour of partially grouted masonry shear walls. Advances in Structural Engineering. 2010.
[4] Shrive NG, Page AW, Simundic G, Dhanasekar M. Shear tests on wide-spaced partially reinforced squat masonry walls. Canadian Masonry Symposium (2009: Toronto,On). [Toronto, Canada]2009.
[5] Calderini C, Cattari S, Lagomarsino S. The use of the diagonal compression test to identify the shear mechanical parameters of masonry. Construction and Building Materials. 2010;24(5):677-85.
[6] Corradi M, Tedeschi C, Binda L, Borri A. Experimental evaluation of shear and compression strength of masonry wall before and after reinforcement: Deep repointing. Construction and Building Materials. 2008;22(4):463-72.
[7] Ismail N, Petersen RB, Masia MJ, Ingham JM. Diagonal shear behaviour of unreinforced masonry wallettes strengthened using twisted steel bars. Construction and Building Materials. 2011;25(12):4386-93.
[8] Petersen RB, Ismail N, Masia MJ, Ingham JM. Finite element modelling of unreinforced masonry shear wallettes strengthened using twisted steel bars. Construction and Building Materials. 2012;33(0):14-24.
[9] Borri A, Castori G, Corradi M, Speranzini E. Shear behavior of unreinforced and reinforced masonry panels subjected to in situ diagonal compression tests. Construction and Building Materials. 2011;25(12):4403-14.
[10] Gabor A, Ferrier E, Jacquelin E, Hamelin P. Analysis and modelling of the in-plane shear behaviour of hollow brick masonry panels. Construction and Building Materials. 2006;20(5):308-21.
[11] Lourenço PB, Rots JG. Multisurface interface model for analysis of masonry structures. J Eng Mech. 1997;123(7):660-8.
[12] Gambarota L, Lagomarsino S. Damage models for the seismic response of brick masonry shear walls. Part II: the continuum model and its applications. Earthq Eng Struct Dyn. 1997;26:441-62.
[13] van Zijl G. Modeling Masonry Shear-Compression: Role of Dilatancy Highlighted. Journal of Engineering Mechanics. 2004;130(11):1289-96.
[14] Sousa R, Sousa H, Guedes J. Diagonal compressive strength of masonry samples—experimental and numerical approach. Materials and Structures. 2013;46(5):765-86.
[15] MSJC. "Building code requirement for masonry structures.". ACI 530/ASCE 5, TMS 402, American Concrete Institute, Detroit.2008.
[16] AS3700. Australian standard for masonry structures. Standard Australian International; 2011.
[17] CSA:S304.1-04. Design of masonry structures. Canadian Standards Association; 2004.
[18] NZS-4230. Design of reinforced concrete masonry structures. New Zealand Standards; 2004.
[19] Shing PB, Schuller M, Hoskere VS. In-plane resistance of reinforced masonry shear walls. Journal of Structural Engineering. 1990;116(3):619-40.
[20] Matsumura A. "Shear strength of reinforced masonry walls". 9th World Conf on Earthquake Engineering. Tokyo1988. p. 121-6.

[21] Haider W. In-plane response of wide spaced reinforced masonry shear walls. [PhD]. Australia Central Queensland University. ; 2007.
[22] Dhanasekar M, Haider W. On the inplane shear and simplified design provisions for reinforced masonry in AS3700. Australian Structural Engineering Conference. Melbourne, Australia: The Meeting Planners; 2008. p. [133]-[45].
[23] Mosele F, da Porto F, Modena C. Reinforced clay masonry walls: effectiveness of reinforcement and shear equations. 11th Canadian Masonry Symposium. Toronto, Ontario2009.
[24] Nolph SM, ElGawady MA. Static Cyclic Response of Partially Grouted Masonry Shear Walls. Journal of Structural Engineering. 2011;138(7):864-79.
[25] ASTM-E519-02. Standard Test Method for Diagonal Tension (Shear) in Masonry Assemblages. ASTM E 519 – 022002.
[26] Abaqus. Abaqus Verification Manual. 2012.
[27] Samarasinghe W, Page A, Hendry A. Behaviour of brick masonry shear walls. STRUCT ENG Struct Eng. 1981;59(3):42.
[28] Dhanasekar M. The performance of brick masonry subjected to inplane loading. Australia: University of Newcastle; 1985.
[29] Seim W. Numerical modeling of the failure of biaxially loaded masonry walls with consideration of anisotropy. Karlsruhe, Germany: University of Karlsruhe; 1994.
[30] Lourenço P, Rots J, Blaauwendraad J. Continuum Model for Masonry: Parameter Estimation and Validation. Journal of Structural Engineering. 1998;124(6):642-52.
[31] Lourenço PB. Computational strategies for masonry structures. Delft University, Netherlands Delft university press; 1996.
[32] Dhanasekar M, Haider W. Explicit finite element analysis of lightly reinforced masonry shear walls. Computers & Structures. 2008;86(1-2):15-26.
[33] Van der Pluijm R. Non-linear behaviour of masonry under tension. Heron-English edition. 1997;42:25-54.
[34] Ganz H, Thürlimann B. Tests on the biaxial strength of masonry. Rep No 7502. 1982;3.
[35] Lurati F, Thürlimann B. Tests in concrete masonry walls. Report; 1990.
[36] Voon KC, Ingham JM. Design Expression for the In-Plane Shear Strength of Reinforced Concrete Masonry. Journal of Structural Engineering. 2007;133(5):706-13.